Chapter 2

Hydrodynamic models

In the last chapter, we developed the OptiMorph model. In this version, the code only works with a local hydrodynamic model (shaoling). This hydrodynamic model has its limitations. In this chapter, we review the literature on existing hydrodynamic models. Next, we look at several types of hydrodynamic model, with a view to incorporating them into our OptiMorph code. These models are XBeach, SWAN, REF/DIF and Shallow-Water. Another model based on the shoaling criterion is developed, and these models are tested on well-known configurations, namely LIP-1C and open-sea simulations.

Current chapter contents

1 Introduction

Coastal hydrodynamics is an important field of research, as it has major implications for coastal engineering, oceanography, and marine ecology. In order to accurately simulate the complex physical processes that occur in coastal waters, numerical models have become increasingly important.

The governing equations that best represent the coastal hydrodynamic processes are the Navier-Stokes equations, which describe the conservation of momentum in a fluid. These equations can be used to model the flow of water in coastal regions, including wave propagation, sediment transport, and water circulation. In addition, the equations can be used to calculate the forces acting on the water, such as the Coriolis force and the drag force. However, these equations are far too complex and are therefore rarely used as is. Some rather heavy models like CROCO (Marchesiello et al. 2021) use the Reynolds-averaged Navier–Stokes equations (RANS) but most of the models are derivatives of the Navier-Stokes equations like the well known Shallow-Water equation.

The first hydrodynamic models were based on linear wave theory (Dean et al. 2004). It is a concept that describes waves thanks to certain quantities: the dispersion, the group velocity and the wave action conservation. It has the advantage of giving an explicit general solution.

Nowadays, we have two major analyses: wave-wave analysis and spectral analysis. Wave-wave analysis is particularly adapted for studies focusing on phenomena linked to celerity thresholds or surface-curve like the wave breaking. In the opposite the spectral approach is more adapted for wave forecasting. We will focus mainly on those with spectral resolution that allows us to obtain directly an averaged water height H name H_s or $H_{1/3}$. On a larger scale, we find oceanographic ocean modelling models that solve the primitive ocean equations with models like NEMO (Breivik et al. 2015) or ROMS (Shchepetkin et al. 2005).

The aim of this chapter is to highlight various hydrodynamic models so that they can be exported to the morphodynamic model in chapter **3**. It begins with an overview of the physic of waves and a discussion of what type of model can be a relevant choice for our morphodynamic model. These hydrodynamic models must produce a significant height H_s as output. They can be temporal or spectral. In order to verify their validity, we will test them on a known benchmark, namely LIP11D (Table **S.6**) (Roelvink et al. 1995). We will also perform simulations on open sea configurations on linear, convex and concave seabed. These will also be performed in the next chapter **3** on morphodynamic aspects.

2 Physics of Wave Motion

This section introduces the mathematical background of wave fluid motion analysis. With the figure below,

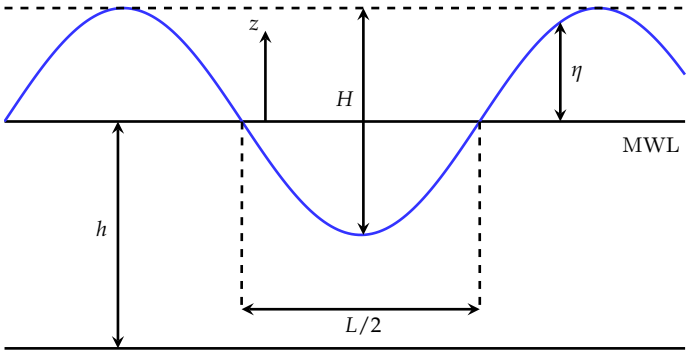

Figure 2.1 – Diagram of the linear theory

The variation of surface elevation with time, from the still water level, is denoted by η and given by:

$$\eta = \frac{H}{2}\cos\left(\frac{x}{L} - \frac{t}{T_0}\right) \tag{2.1}$$

with the hydrodynamic notations as follows:

- H the wave height (m),
- T_0 the wave period (s),
- L the wave length (m),
- θ the direction (rad),
- $k = 2\pi/\mathrm{L}$ the wavenumber (m^{-1}),
- a the wave amplitude, $a = H/2$ (m),
- ka the wave slope (1),
- h the water depth (m),
- $\bar{\eta}$ the mean free surface level (m),
- $D = h + \bar{\eta}$ the local water depth (m).

We then introduce the Eulerian notations with the position with the horizontal vector having two components $\mathbf{x} = (x, y)$ and the vertical position z. Celerities are their respective temporal derivatives denoted $\mathbf{u} = (u, v)$ and w.

The equation that perfectly governs the motion of water and therefore of a wave is the Navier-Stockes equation:

$$\begin{cases} \dfrac{\partial \mathbf{u}}{\partial t} + \mathbf{u} \cdot \nabla \mathbf{u} + w \dfrac{\partial \mathbf{u}}{\partial z} = -\dfrac{1}{\rho_w} \nabla p + \nu \left(\nabla^2 \mathbf{u} + \dfrac{\partial^2 u}{\partial z^2} \right), & \text{(2.2a)} \\ \dfrac{\partial w}{\partial t} + \mathbf{u} \cdot \nabla w + w \dfrac{\partial w}{\partial z} = -g - \dfrac{1}{\rho_w} \dfrac{\partial p}{\partial z} + \nu \left(\nabla^2 w + \dfrac{\partial^2 w}{\partial z^2} \right), & \text{(2.2b)} \\ \nabla \cdot \mathbf{u} + \dfrac{\partial w}{\partial z} = 0, & \text{(2.2c)} \end{cases}$$

with ρ_w the water density, ∇ the horizontal gradient, ν the viscosity, g the gravity constant, p the pressure, $\mathbf{u} = (u, w)$ is a velocity vector of x and y components. The equation (2.2a), (2.2b) are the momentum equations and the equation (2.2c) is the continuity equation. We could simplify these equations using some assumptions:

- The pressure is uniform $\Longrightarrow -\frac{1}{\rho_w} \nabla p = 0$ and $\frac{\partial p}{\partial z} = 0$,
- The density is constant $\Longrightarrow \rho_w = cte$,
- The bottom is horizontal $\Longrightarrow \frac{\partial}{\partial x} = cte$,
- The fluid is incompressible $\Longrightarrow \nabla \cdot v = 0$,
- The fluid is non-viscous $\Longrightarrow \nu = 0$,
- The fluid is irrotational $\Longrightarrow \mathbf{u} = \nabla \phi$ and $w = \frac{\partial \phi}{\partial z}$.

By neglecting the viscosity, we obtain the Euler (1752) equations:

$$\begin{cases} \dfrac{\partial \mathbf{u}}{\partial t} + \mathbf{u} \cdot \nabla \mathbf{u} + w \dfrac{\partial \mathbf{u}}{\partial z} = -\dfrac{1}{\rho_w} \nabla p, & \text{(2.3a)} \\ \dfrac{\partial w}{\partial t} + \mathbf{u} \cdot \nabla w + w \dfrac{\partial w}{\partial z} = -g - \dfrac{1}{\rho_w} \dfrac{\partial p}{\partial z}, & \text{(2.3b)} \\ \nabla \cdot \mathbf{u} + \dfrac{\partial w}{\partial z} = 0, & \text{(2.3c)} \end{cases}$$

that can be express in vectorial form:

$$\frac{\partial \vec{V}}{\partial t} + \left(\vec{V} \cdot \nabla \right) \vec{V} = -\frac{1}{\rho_w} \nabla P - g\vec{k} \tag{2.4}$$

with $\vec{V} = (u, v, w)$ and P the vector of each pressure component in (x, y, z) and $\vec{k} = (0, 0, 1)$. Using vector calculus, we have:

$$\nabla(\vec{V}\cdot\vec{V}) = 2\vec{V}\cdot \underbrace{\cancel{(\vec{\nabla}\cdot\vec{V})}}_{\text{incompressible}} + 2(\vec{V}\cdot\nabla)\vec{V},$$

$$(\vec{V}\cdot\nabla)\vec{V} = \frac{1}{2}\nabla(\vec{V}\cdot\vec{V}),$$

and then, replacing the potential $\vec{V} = \nabla\phi'$, Euler (1752) equation becomes:

$$\frac{\partial\nabla\phi'}{\partial t} + \frac{1}{2}\nabla\left(\nabla\phi'\cdot\nabla\phi'\right) = -\frac{1}{\rho_w}\nabla P - g\vec{k}, \tag{2.5}$$

however, we have: $\nabla(gz) = g\vec{k}$, then:

$$\nabla\left(\frac{\partial\phi'}{\partial t} + \frac{1}{2}\left(\nabla\phi'\cdot\nabla\phi'\right)\right) = -\nabla\left(\frac{P}{\rho_w} - gz\right), \tag{2.6}$$

by integrating, making a change of variable between ϕ' and ϕ, we obtain the classical Bernouilli energy equation:

$$\frac{\partial\phi}{\partial t} + \frac{1}{2}\left[|\nabla\phi|^2 + \left(\frac{\partial\phi^2}{\partial z}\right)\right] + \frac{p}{\rho_w} + g\eta = C(t), \quad z = \eta \tag{2.7}$$

with $C(t)$ a function depending on time which will be considered as null. Making the assumptions that $H \ll L$ and $H \ll h$ results in the linearized boundary conditions (in which the smaller, higher order and product terms are neglected). The resulting kinematic and dynamic boundary equations are then applied at the still water level, given by,

$$w = \frac{\partial\eta}{\partial t}, \quad g\eta + \frac{\partial\phi}{\partial t}, \quad z = 0. \tag{2.8}$$

The resulting solution for ϕ is given by:

$$\phi = -g\int\eta(t)dt \tag{2.9}$$

which gives us with the equation of η (**2.22a**):

$$\phi = -gH\frac{T_0}{4\pi}\frac{\cosh\left[\left(\frac{2\pi}{L}\right)(h+z)\right]}{\cosh\left[\left(\frac{2\pi}{L}\right)h\right]}\sin\left(\frac{2\pi x}{L} - \frac{2\pi t}{T_0}\right). \tag{2.10}$$

We can state that the condition of continuous surface celerities is

$$w = \frac{\partial \phi}{\partial z} = \mathbf{u} \cdot \nabla \eta + \frac{\partial \eta}{\partial t} = \nabla \phi \cdot \nabla \eta + \frac{\partial \eta}{\partial t}, \quad \text{for} \quad z = \eta \tag{2.11}$$

and that (2.2c) becomes equivalent to the Laplace equation for ϕ :

$$\nabla \cdot \mathbf{u} + \frac{\partial w}{\partial z} = \nabla^2 \phi + \frac{\partial^2 \phi}{\partial z^2} = 0, \quad \text{for} \quad -h \leq z \leq \eta \tag{2.12}$$

and for a horizontal bottom the equation of continuous vertical velocity is

$$w = \frac{\partial \phi}{\partial z} = 0, \quad \text{for} \quad z = -h. \tag{2.13}$$

Additionally, after a few manipulations on (2.3a) and (2.3b) we obtain the beginning of a wave equation:

$$\frac{\partial^2 \phi}{\partial t^2} + g\frac{\partial \phi}{\partial z} = g\nabla\phi \cdot \nabla\eta - \frac{1}{2}\frac{\partial \eta}{\partial t}\frac{\partial^2 \phi}{\partial z \partial t} - \left(\frac{\partial}{\partial t} + \frac{\partial \eta}{\partial t}\frac{\partial}{\partial z}\right)\left[\nabla\phi \cdot \nabla\phi + \left(\frac{\partial \phi^2}{\partial z}\right)\right] + C(t), \text{ for } z = \eta \tag{2.14}$$

3 Linear Wave Theory

The notion of uniform motion (linear motion of a wave) must respect certain assumptions: the wave slope is small ($ka \ll 1$), the quantity a/D is small too: ($a/D \ll 1$). These are small-amplitude waves

Regarding the small-amplitude waves assumptions: ($ka \ll 1$) and ($a/D \ll 1$). We know that it has been proved that the non-linear term of equation (2.14) can be ignored and that from a first order Taylor development to get equation (2.14) for $z = 0$ instead of $z = \eta$, the linearized wave equation is now:

$$\boxed{\frac{\partial^2 \phi}{\partial t^2} + g\frac{\partial \phi}{\partial z} = 0}, \quad \text{for} \quad z = 0. \tag{2.15}$$

From a Fourier decomposition, then replacing the solution into the Laplace equation equation (2.12) and taking into account the bottom boundary condition, we obtain the relation

$$\frac{\partial^2 \Phi}{\partial t^2} + gk \tanh(kD)\Phi = 0 \tag{2.16}$$

with the solution:

$$\Phi(t) = \mathcal{R}\left(\Phi_{\mathbf{k}} e^{-i\sigma t}\right) \tag{2.17}$$

which give the dispersion relation given by Laplace,

$$\sigma^2 = gk \tanh(kD) \tag{2.18}$$

with the wave length L, wave period T_0, $\sigma = 2\pi/T_0$ and $k = 2\pi/L$. By replacing, we obtained:

$$\left(\frac{2\pi}{T_0}\right)^2 = g\frac{2\pi}{L}\tanh kh. \tag{2.19}$$

We introduce elevation surface phase as:

$$\Theta = \mathbf{k}\cdot\mathbf{x} - \sigma t + \Theta_0 \tag{2.20}$$

with $0 \leq \Theta_0 \leq 2\pi$ the phase shift and a the amplitude

$$a = i\frac{\sigma}{g}\Phi_{\mathbf{k}} \tag{2.21}$$

the solution is of Airy (1845) wave for free surface elevation are:

$$\eta = a\cos\Theta, \tag{2.22a}$$

$$\mathbf{u} = a\frac{\mathbf{k}}{k}\sigma\frac{\cosh(kz+kh)}{\sinh(kD)}\cos\Theta, \tag{2.22b}$$

$$w = \sigma\frac{\cosh(kz+kh)}{\sinh(kD)}\sin\Theta, \tag{2.22c}$$

$$p = \bar{p}^H + \rho_w g a\frac{\cosh(kz+kh)}{\cosh(kD)}\cos\Theta, \tag{2.22d}$$

where the mean hydrostatic pressure $\bar{p}^H = -\rho_w g(z-\bar{\eta}) + \bar{p}_a$ with p_a being the atmospheric pressure. These is the linear approach of the wave propagation.

After Airy's Works, Stokes (1847) extended the Airy's solution to take into account the neglected non-linear terms in equation (**2.14**). Even if the latter improves the fit with actual observations of waves, the Airy's solution is a reliable approximation for deep-bottom wave propagation which is almost irrotational, without being so far from the reality to the coast on wave-breaking zones.

In order to demonstrate shoaling we must make two assumptions:

- Period is the variant of propagation and remains constant as depth changes;

- The energy remains constant until it reaches breaking up.

3.1 Celerity

Substituting this solution for ϕ equation (2.10) into the two linearized surface boundary conditions yields the surface profile given in Equation equation (2.22a) and the wave celerity C given by:

$$\boxed{C = \frac{gT_0}{2\pi}\tanh(\frac{2\pi h}{L}) = C_0\tanh(kh)} \tag{2.23}$$

where $C_0 = g/\omega$, $\omega = 2\pi/T_0$ and $k = 2\pi/L$.

3.2 Wave Energy

We have the potential and kinetic energy called E_i with the integration and L: the wave length:

$$E_i = \frac{1}{L}\left(2\int_0^L(\rho g\eta dx)\frac{\eta}{2}\right) = \frac{1}{16}\rho g H^2 \tag{2.24}$$

which gives us both the formulation:

- Potential energy: $E_p = \frac{1}{16}\rho g H^2$
- Kinetic energy: $E_c = \frac{1}{16}\rho g H^2$

And then the total wave energy:

$$\boxed{\mathcal{E}_{\mathcal{H}} = \frac{1}{8}\rho g H^2} \tag{2.25}$$

One might expect that wave power (or the rate of transmission of wave energy) would be equal to wave energy times the wave celerity. This is incorrect, and the derivation of the equation for wave power leads to an interesting result which is of considerable importance. Wave energy is transmitted by individual particles which possess potential, kinetic and pressure energy. Summing these energies and multiplying by the particle velocity in the x-direction for all particles in the wave gives the rate of transmission of wave energy or wave power (P), and leads to the result (for an Airy (1845) wave)

$$P = \frac{\rho g H^2}{8}\frac{C}{2}\left(1 + \frac{2kh}{\sinh 2kh}\right) = EC_g \tag{2.26}$$

where C_g is the group wave celerity, given by

$$\boxed{C_g = \frac{C}{2}\left(1 + \frac{2kh}{\sinh 2kh}\right).} \tag{2.27}$$

In deep water ($h/L > 0.5$) the group wave velocity $C_g = C/2$, and in shallow-water $C_g = C$. Hence, in deep water wave energy is transmitted forward at only half the wave celerity.

3.3 Shoaling Coefficient

Therefore, we can say that the offshore flow of energy will be constant in its propagation until it comes to breaking near shore. We call $\mathcal{E}_{F0}$ the offshore flow and $\mathcal{E}_{Fh}$ the flow relative to depth h. Thus:

$$\mathcal{E}_{F0} = \mathcal{E}_{Fh}$$

and thus

$$\mathcal{E}C_{g_0} = \mathcal{E}C_g$$

Where: C_{g_0} is the group velocity offshore and C_g is the group velocity relative to the depth H. Considering that $C_{g_0} \neq C_g$, we have with (2.25):

$$\rho g \frac{H_0^2}{8} \cdot C_{g_0} = \rho g \frac{H^2}{8} \cdot C_g \rightarrow \frac{H^2}{H_0^2} = \frac{C_{g_0}}{C_g}$$

This ratio is called the shoaling coefficient:

$$K_s^2 = \frac{H^2}{H_0^2} = \frac{C_{g_0}}{C_g} \rightarrow K_s = \sqrt{\frac{C_{g_0}}{C_g}}.$$

Thanks to the equations (2.27), (2.23) and $C_{g_0} \underset{h\to+\infty}{\longrightarrow} \frac{C_0}{2}$, we deduce:

$$\boxed{K_S = \left[\tanh(kh)\left(1 + \frac{2kh}{\sinh(2kh)}\right)\right]^{-1/2}.} \tag{2.28}$$

This coefficient allows us to use the Shoaling model (1.2a) in a very simplistic approach of our model. This model will be improved in the extended version of the following part 3.4.

3.4 Extended Shoaling Model

The Shoaling model 1.7 did not succeed to model wave breaking with wave periods $T_0 > 2\,s$. This model was therefore improved to give birth to the extended model below:

Extended Shoaling model

$$H(x,t) = \begin{cases} H_0(x,t)K_S(x,t) & \text{for } x \in \Omega_S \quad (2.29a) \\ \mathcal{F}\left(\gamma h(x,t)\right) & \text{for } x \in \Omega_B \quad (2.29b) \end{cases}$$

where $\mathcal{F}$ is a numerical parameterization function of the breaking defines below (5.3):

$$\mathcal{F}\left(\gamma h(x,t)\right) = H(x_{start}) + \left[H(x_{stop}) - H(x_{start})\right] \cdot f\left(\frac{x - x_{start}}{x_{stop} - x_{start}}\right) \cdot g\left(\frac{h_{max} - h}{h_{max} - h_{min}}\right) \quad (2.30)$$

with $x \in \Omega_B = [x_{start}, x_{stop}]$, $h \in [h_{min}, h_{max}]$ and the following notations:

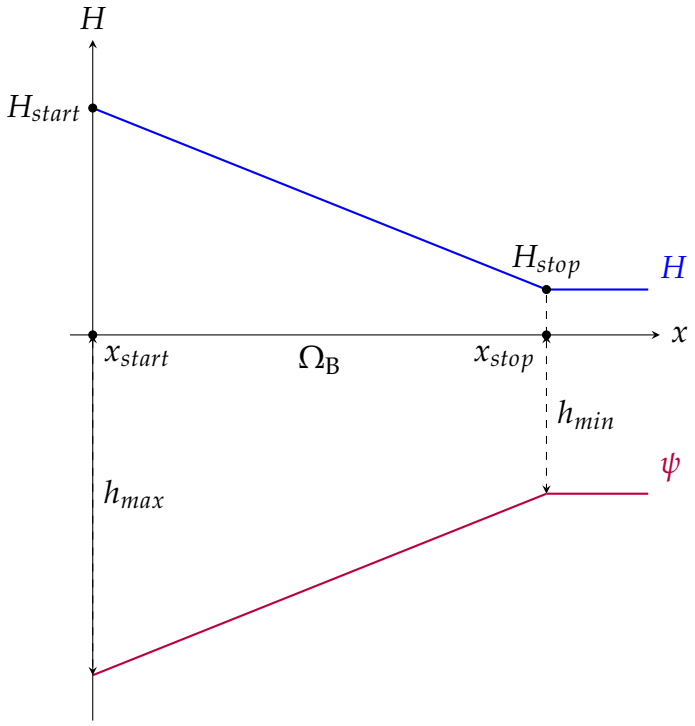

Figure 2.2 – Illustration of notations.

H_{start} and H_{stop} are the water heights at the beginning and end of the breaking on the

domain $\Omega_B = [x_{start}, x_{stop}]$. The first function f gives an account of breaking without taking into account the bed shape. It simply gives the appearance of breaking. The second function g takes into account the seabed and interacts with it. Note that if f and g are the affine functions $x \longmapsto x$, we find the breaking $\gamma h(x,t)$ illustrated on figure 5.2. We can present below (figure 5.3) some of these functions that set the breaking:

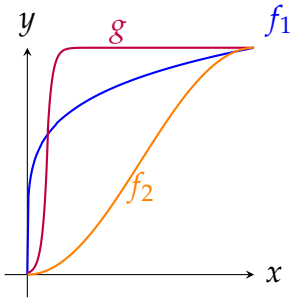

Figure 2.3 – Illustration of f_1, f_2 and g defined in $[0,1] \longrightarrow [0,1]$.

These functions were chosen to try to capture a natural breaking. They have no physical meaning.

It is necessary to stipulate that the model will first locate all the Ω_B domains and then apply the equation (5.3) on each of them.

This type of model gives us the following breaking for a simulation with a wave period $T_0 = 10\,s$ and an offshore water height of $H_0 = 2\,m$.

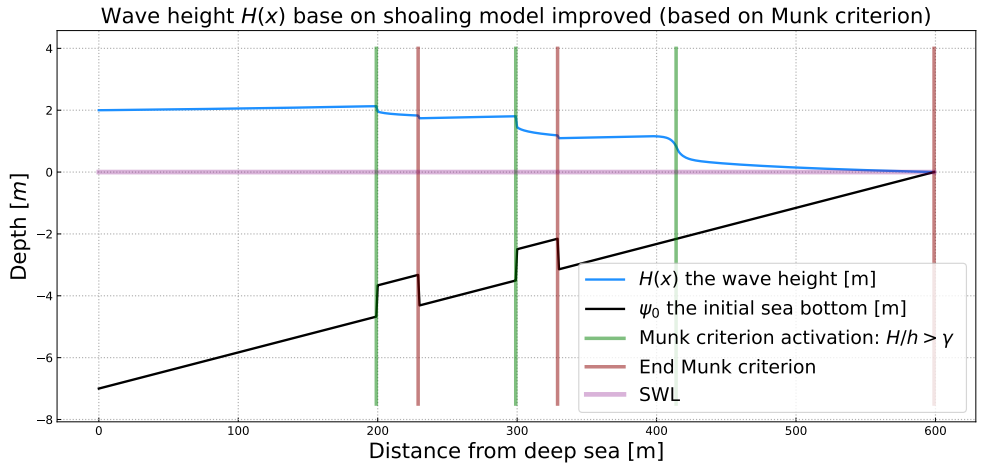

Figure 2.4 – Wave height $H(x)$ with the Shoaling model with the last improve (using f and g) for a configuration with a linear sea bottom of slopes about 0.11, wave period $T_0 = 10\,s$ and offshore water height of $H_0 = 2\,m$.

This breaking uses the function $f : x \longmapsto x^{\frac{1}{5}}$ but it can be changed to the desired shape.

4 Wave Resolving

4.1 Context

The alternative method of resolving phases for shallow water waves often relies on Boussinesq-type (BT) equations, with notable contributors including (Peregrine 1967; Freilich et al. 1984; Madsen et al. 1992; Liu et al. 2002). The mild-slope equation, as proposed by Berkhoff (1972), is also commonly used as a port agitation model. It can be used to isolate the eigen modes of vibration within it. These models aim to reconstruct the sea surface's characteristics in both space and time, encompassing horizontal and vertical flow velocity. They inherently account for phenomena like refraction, diffraction, and, in some instances, triad and quadruplet wave interactions. Dissipation processes, such as bottom friction and depth-induced wave breaking, can be parameterized in these models. However, they do not incorporate wind-induced wave generation.

Despite these models' effectiveness in capturing vital coastal and nearshore wave phenomena, numerical models based on BT equations have grown indispensable in the field of coastal engineering, as highlighted by Rusu et al. (2012). The standard BT equations for variable water depths were initially formulated by Peregrine (1967), though they were limited to addressing weakly non-linear and weakly dispersive shallow water flows. To address this limitation, Madsen et al. (1991) and Nwogu (1993) expanded upon the standard BT equations, creating a practical tool for simulating the non-linear transformation of irregular, multi-directional waves in varying water depths before wave breaking occurs.

The most advanced BT models are versatile, applicable in both deep and shallow waters, as well as when dealing with highly non-linear waves. However, one limitation of traditional BT models is their inability to accurately describe the overturning and turbulence generation during wave breaking. Researchers have consequently developed semi-empirical approaches to address these challenges.

Widely used in the coastal community, depth-integrate models are very popular because ; i) They are a simpler set of equations than the full three-dimensional ones, and so allow for a much more straightforward analysis of sometimes complex problems ; ii) In spite of their simplicity, the equations provide a reasonably realistic representation of a variety of phenomena in atmospheric and oceanic dynamics. As these models are vertically integrated, it is assumed that they cannot model transfers between horizontal layers. Some models, such as the Shallow-Water (SW) model (Marche et al. 2007), neglect dispersion

$$\mu = \frac{H_0^2}{\lambda^2} \ll 1, \tag{2.31}$$

and remain easy to solve numerically. Other more advanced models, such as Green-Naghdi (GN), Serre-Green-Naghdiand (SGN) KdV (Kim et al. 2001), take dissipation into account but are numerically difficult to solve.

In our work, we'll be using the most popular model, the Shallow-Water model (Marche

et al. 2007) and the REF/DIF model (James Thornton Kirby et al. 1994).

4.2 Derivation of Shallow-Water Model

Taking back the equation Euler equation (2.4), we consider the 1D Euler's equations without surface tension:

$$\begin{cases} \text{free surface condition}: \ p = 0, \quad \dfrac{\mathrm{D}h}{\mathrm{D}t} = \dfrac{\partial h}{\partial t} + u\dfrac{\partial h}{\partial x} = w, \quad \text{on } z = h(x,y,t) & \text{(2.32a)} \\ \text{momentum equation}: \ \dfrac{\partial u}{\partial t} + u\dfrac{\partial u}{\partial x} + \dfrac{1}{\rho_w}\dfrac{\partial P}{\partial x} + gz = 0 & \text{(2.32b)} \\ \text{continuity equation}: \ \dfrac{\partial u}{\partial x} = 0, & \text{(2.32c)} \\ \text{bottom boundary condition}: \ u\dfrac{\partial z}{\partial x} = 0, \quad \text{on } z = 0. & \text{(2.32d)} \end{cases}$$

Here, p is the pressure, h the vertical displacement of the free surface, u the x velocity, ρ_w the density, g the acceleration due to gravity. (Figure 2.5).

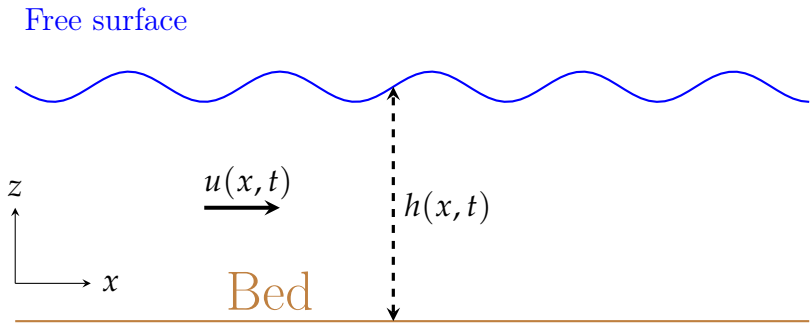

Figure 2.5 – Shallow-Water diagram for a 1D flow.

For the first step of the derivation of the shallow-water equations, we consider the global mass conservation. We integrate the continuity equation (2.32c) vertically as follows,

$$\begin{aligned} 0 &= \int_0^h \frac{\partial u}{\partial x}\mathrm{d}z & \text{(2.33a)} \\ &= \frac{\partial}{\partial x}\int_0^h u \ \mathrm{d}z - u|_{z=h}\frac{\partial h}{\partial x}, & \text{(2.33b)} \end{aligned}$$

where the bottom boundary condition (2.32d) was used in the fourth row. With the surface condition (2.32a), equation (2.33b) becomes

$$\frac{\partial h}{\partial t} + \frac{\partial}{\partial x}\int_0^h u \, \mathrm{d}z = 0 \tag{2.34}$$

In the following stage, we proceed with the long-wave approximation, where we consider the wavelength to be significantly greater than the fluid's depth. It's important to note that we do not make any assumptions regarding the perturbations of having small amplitudes, ensuring that non-linear terms are accounted for rather than being disregarded. By employing the long-wave approximation, we can derive the hydrostatic pressure by performing an integration of the vertical component of the momentum equation.

$$\int_z^h \frac{\partial p}{\partial z} \, \mathrm{d}z = -\int_z^h \rho g \, \mathrm{d}z \tag{2.35a}$$

$$p(x,h,t) - p(x,z,t) = -\rho g(h(x,t)) - z) \tag{2.35b}$$

$$p(x,z,t) = \rho g(h(x,t) - z). \tag{2.35c}$$

We applied the surface condition represented as $p(x,h,t) = 0$. Utilizing this equation for the hydrostatic pressure (2.35c) and additionally supposing that there are no vertical variations in the parameter u ($\Rightarrow$ equation (2.32a) $= 0$), the horizontal momentum equations of the shallow-water system can be derived in the following manner:

$$\partial_t u + u\partial_x u + g\partial_x h = 0. \tag{2.36}$$

The conservation of mass given by (2.34) becomes

$$\partial_t h + \partial_x(hu) = 0. \tag{2.37}$$

Then, equations (2.36) and (2.37) are the shallow-water equations. More details on the derivation are available on (Fabien Marche 2007).

4.3 Shallow-Water Equations with Variable Bottom

Previously, we presented the flat-bottomed Shallow-Water model. However, our model requires a variable-bottom hydrodynamic model. Indeed, our model runs a large number of simulations with different geometries before completing. It is therefore essential that the model can run a hydrodynamic simulation on any bottom. A variable bottom on the Shallow-Water model adds an additional source term and complexity to the numerical implementation. The hyperbolic system of equations (2.36) and (2.37) thus becomes:

$$\partial_t h + \partial_x q = 0 \tag{2.38a}$$

$$\partial_t q + \partial_x \left(\frac{q^2}{h} + \frac{1}{2} g h^2 \right) = -g h \partial_x Z \tag{2.38b}$$

$$+ \text{ Boundary condition,} \tag{2.38c}$$

with h he water height, u the velocity and $q = hu$ the flow. We use the notation $d_i = \frac{\partial}{\partial i}$. These quantities are presented in figure 2.6.

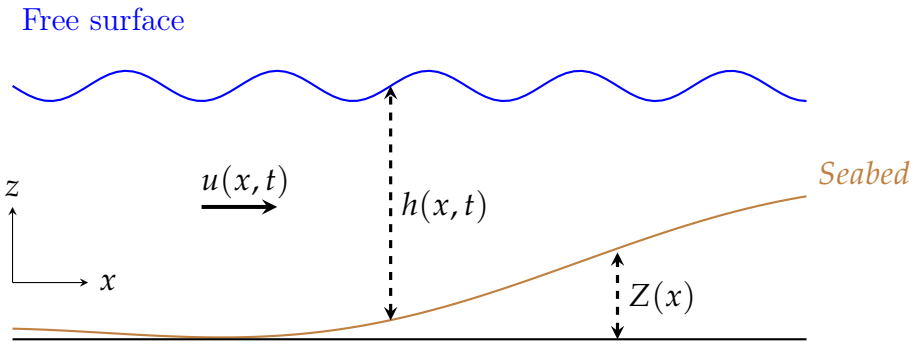

Figure 2.6 – Shallow-Water diagram for a 1D flow and variable bottom.

The equation (2.38a) represents the continuity. The second (2.38b) is the moment and the third the boundary conditions. Generally, the resolution of these equations is done using the finite volume method. Although the addition of source terms (variable background (Berthon et al. 2018; Marche et al. 2007), Exner coupling (Serrano-Pacheco et al. 2012), ...) makes the resolution more complex, the resolutions remain mainly on this principle. In our case, we use finite volume solving with a VFRoe numerical scheme from (Marche et al. 2007).

4.4 REF/DIF Numerical Model

REF/DIF is a phase-resolving parabolic refraction-diffraction model for ocean surface wave propagation. It was originally developed by Jim Kirby and Tony Dalrymple starting in 1982, based on Kirby's dissertation work. This work led to the development of REF/DIF 1, a monochromatic wave model (James Thornton Kirby et al. 1994).

This model is solving the Berkhoff (1972) equation, known as the mild slope equation. It is written in terms of the surface displacement, $\eta(x, y)$. The equation, in terms of horizontal gradient operator, is

$$\nabla_h \cdot \left(C C_g \nabla_h \eta \right) + \sigma^2 \frac{C_g}{C} \eta = 0 \tag{2.39}$$

where C and C_g are defined in (2.27) and (2.23).

In contrast to the mild slope model which is valid for varying bathymetry, researchers in the area of wave diffraction were developing models for constant bottom applications. For example, Mei et al. (1980) developed a simple parabolic equation for wave diffraction and applied it to the diffraction of waves by a slender island. Their equation is

$$\frac{\partial A}{\partial x} = \frac{i}{2k}\frac{\partial^2 A}{\partial y^2}$$

where A is a complex amplitude related to the water surface displacement by

$$\eta = Ae^{i(kx-\sigma t)}.$$

Yue et al. (1980), using a multiple scales approach, developed a nonlinear form of this equation, which accurately predicts the propagation of a third order Stokes wave.

The parabolic model of REF/DIF, described below, combines the essential features of the two approaches described above. The variable depth features of the mild-slope equation (along with extensions to include effects of wave-current interaction) are retained, but the model is developed in parabolic form and in terms of a complex amplitude A.

$$\left(C_g + U\right) A_x + VA_y + i(\bar{k} - k)\left(C_g + U\right) A + \frac{\sigma}{2}\left\{\left(\frac{C_g + U}{\sigma}\right)_x + \left(\frac{V}{\sigma}\right)_y\right\} A$$
$$- \frac{i}{2\sigma}\left(\left(p - V^2\right) A_y\right)_y - \sigma\frac{k^2}{2} D|A|^2 A = 0$$

where $p = CC_g$ and $\bar{k}$ = reference wave number, taken as the average wave number along the y axis, and U is the mean current velocity in the x coordinate direction and V is in the y direction. The nonlinear term includes D, which is

$$D = \frac{\left(\cosh 4kh + 8 - 2\tanh^2 kh\right)}{8\sinh^4 kh}$$

Finally, James T Kirby (1986a) derived the above equation for a wide-angle parabolic approximation, which allows the study of waves with larger angles of incidence with respect to the x axis. This more precise equation was extended (James T. Kirby 1986b) and used in REF/DIF 1 (James Thornton Kirby et al. 1994).

Note : The mild slope equation, excluding additional terms for bed slopeprovides accurate results for the wave field over bed slopes ranging from 0 to approximately 1/3 (N. Booij

1983). This must be taken into account when using the REF/DIF model.

5 Spectral Wave Resolution

5.1 Context

We define a wave has a height H, a period T, a direction θ, and so forth. modelling wave with statistical is realistic because it has been shown that the N individual wave heights $H_1, H_2, \ldots, H_N$ of a certain time series follows a Rayleigh distribution (Figure 2.7), expressed here with its survival

$$P(H > h) = \mathrm{e}^{-(h/H_{\mathrm{rms}})^2} \tag{2.40}$$

where $H_{rms} = \sqrt{\frac{1}{N}\sum_{i=1}^{N} H_i^2}$ and the H_i denote the individual wave height in a certain time series. The Rayleigh distribution is generally suitable for commonly observed waves. As soon as the waves are quite high, the distribution of Tayfun (1980) must be considered. Tayfun distribution is more realistic since most of the non-linear waves effects are taken into account.

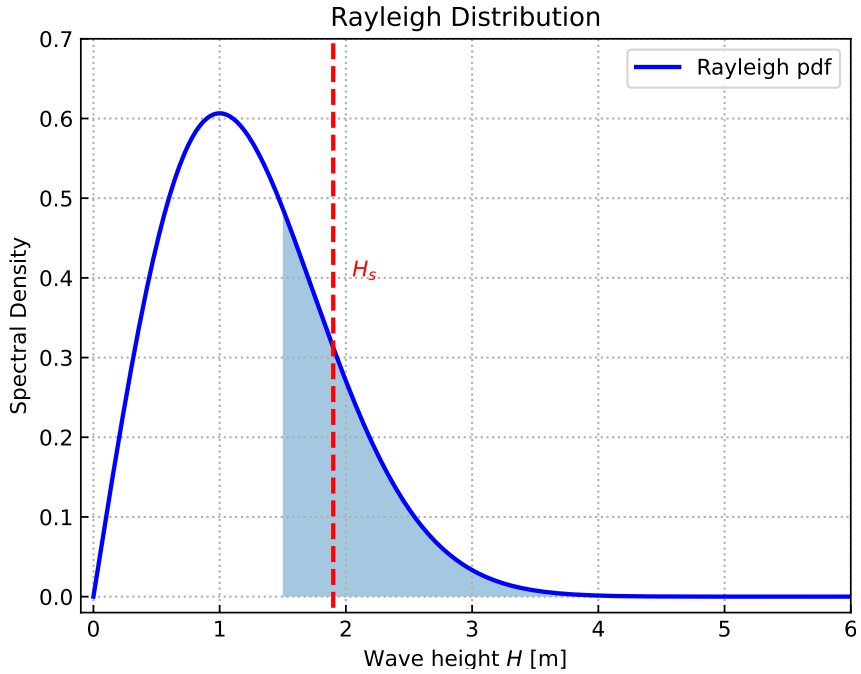

Figure 2.7 – Rayleigh density function $f(H, 1.9)$. The red area is the third highest observed waves in a certain time-series. The dashed line represents $H_{1/3}$, the mean of the third highest observed waves also assimilated to the significant wave height H_s.

With that kind of distribution, a common variable named the significant wave height

H_s is determined. From wave-wave analysis, H_s is defined as $H_{1/3}$: the mean of the third highest waves of the time-series. It corresponds to a sea-state in a stationary condition. Another variable used is $H_{\max}$ which is the maximum wave height observed, it is highly depending on the length of the time series.

5.2 Mathematical Background

An important problem occurs in the analysis of the wave motion when the wave has a length greater than L, which requires the treatment of irregularities. One can use the statistical analyses developed by Fourier (FFT) (Nussbaumer et al. 1982) because the waves are supposed to satisfy the linear wave theory (locally). Indeed, the water level signal can be decomposed into superimposed sinusoidal waves. And thus be decomposed into Fourier series in the form of a given direction α (for simplicity's sake):

$$\eta(x,t) = \sum_{n=0}^{\infty} \eta_n(x) = \sum_{n=0}^{\infty} A_n \cos\left(k_n x + \phi_n\right) \tag{2.41}$$

where A_n denote Fourier's amplitude is associated with a particular frequency k_n and a particular phase shift ϕ_n. The variance of a sinusoidal surface is the average over one wavelength L of the surface elevation squared (assuming that the mean surface is at zero):

$$V(\eta_1) = \frac{1}{L}\int_0^L \left[A \sin\left(\frac{2\pi x}{L}\right)\right]^2 dx = \frac{1}{L}\int_0^L A^2 \left[\frac{1}{2} - \cos\left(\frac{4\pi x}{L}\right)\right] dx = \frac{1}{2}A^2 \tag{2.42}$$

Thus the energy per unit area of a sinusoidal wave can also be written in terms of its variance:

$$\frac{\text{energy}}{\text{area}} = \rho g V(\eta_1). \tag{2.43}$$

We have therefore with (2.42) and (2.41),

$$V(\eta) = \sum_{n=0}^{\infty} \frac{1}{2} A_n^2. \tag{2.44}$$

Now let Δk_n be a frequency interval centered on frequency k_n, whose sinusoidal has amplitude A_n. We then define

$$E\left(k = k_n\right) \equiv \lim_{\Delta k_n \to 0} \frac{\frac{1}{2}A_n^2}{\Delta k_n}. \tag{2.45}$$

In this definition, keep in mind that each A_n is associated with a particular frequency k_n, , and that the limit operation holds for each value of n. We are thus defining a function

of the spatial frequency, which becomes a as the bandwidth Δk_n goes to zero.
The continuous function $E(k)$ is called the omnidirectional elevation variance spectrum. "Omnidirectional" means that there is no reference direction (e.g., a direction of wave propagation relative to the wind direction) included in the quantity. Equations (2.44) and (2.45) show that integrating the omnidirectional variance spectrum over all frequencies gives the total elevation variance:

$$V(\eta) = \left\langle \eta^2 \right\rangle = \int_0^\infty E(k)dk \tag{2.46}$$

which gives us in multi-directional, the well known formula

$$E = \int_0^\infty \int_0^{2\pi} E(k,\theta)\mathrm{d}k\ \mathrm{d}\theta \tag{2.47}$$

of the wavenumber-direction spectrum. Other expressions of the wave spectrum are also used. In particular, wave-lengths and wave frequencies are interrelated via the dispersion equation (2.18) and

$$E(k,\theta)\mathrm{d}k\ \mathrm{d}\theta = E(f,\theta)\mathrm{d}f\ \mathrm{d}\theta. \tag{2.48}$$

The wave density spectrum (i.e. right side of (2.18)) defines the repartition of the wave energy [2] along frequencies and direction. Unlike the signal of the free surface elevation, the density spectrum is relatively regular and allows compressing the information of the full signal.

As recalled in (Tolman et al. 2009), without currents E is a conserved quantity. In case of currents, spectral component is no longer conserved due to the work done by current on the mean momentum transfer of waves. Hence, ones are also interested in using the wave action spectrum A as

$$A(k,\theta) = \frac{E(k,\theta)}{\sigma} \tag{2.49}$$

which is conserved whatever the case (G. á. Whitham 1965). Thanks to that definition, we can express the wave propagation as

$$\frac{DA}{Dt} = \frac{S}{\sigma} \tag{2.50}$$

where A is the action wave spectrum, D/Dt is here the total derivative and S is the net effect of sources and sinks for the wave spectrum E. Since left part of (2.50) considers linear wave propagation as presented before, any perturbing effects are gathered in the expression of S. In the next subsection we identify physical phenomena in charge of the balance of (2.50).

5.3 Interesting Quantity's

The first quantity of interest is generally the significant wave height H_s. From the spectrum we define

$$H_{m0} = 4E^{1/2} = 4\left[\int_0^\infty \int_0^{2\pi} E(f,\theta)\mathrm{d}f\ \mathrm{d}\theta\right]^{1/2}. \tag{2.51}$$

In practice $H_{1/3} \simeq H_{m0}$ (Longuet-Higgins 1963). H_{m0} is therefore the spectral representation of the significant wave height. The denotation $m0$ stands for the zero moment of power spectrum, which is more generally defined for the order p as

$$m_p = \int_0^\infty \int_0^{2\pi} f^p E(f,\theta)\mathrm{d}f\ \mathrm{d}\theta \tag{2.52}$$

Several other quantities often used in ocean engineering derive from the spectrum. In particular, f_p is the peak frequency, with $E\left(f_p\right) = E_{\max}$ and the peak period $T_p = 1/f_p$. Other famous periods $T_{m0,1}, T_{m0,2}$ and $T_{m0,-1}$ stem from the period of order p defined as

$$T_{m0,p} = \left[\frac{\int_0^{f_{\max}} \int_0^{2\pi} f^p E(f,\theta)\mathrm{d}f\ \mathrm{d}\theta}{\int_0^{f_{\max}} E(f)\mathrm{d}f}\right]^{-1/p} \tag{2.53}$$

with $f_{\max}$ the highest frequency observed. Finally, if we define

$$a_1(f) = \int_0^{2\pi} E(f,\theta)\cos\theta\mathrm{d}\theta \Big/ \int_0^{2\pi} E(f,\theta)\mathrm{d}\theta, \tag{2.54a}$$

$$b_1(f) = \int_0^{2\pi} E(f,\theta)\sin\theta\mathrm{d}\theta \Big/ \int_0^{2\pi} E(f,\theta)\mathrm{d}\theta, \tag{2.54b}$$

then the mean wave direction for the frequency f is

$$\theta_m(f) = \arctan\left(\frac{b_1(f)}{a_1(f)}\right). \tag{2.55}$$

In particular, $\theta_m\left(f_p\right)$ is the main wave direction (or peak wave direction). Ones are also interested in the mean wave direction θ_M defined by integrating over the direction as

$$\theta_M = \arctan\left(\frac{\int_0^\infty b_1(f)\mathrm{d}f}{\int_0^\infty a_1(f)\mathrm{d}f}\right). \tag{2.56}$$

To reconstruct the signal from a statistical approach as detailed here is valid in mostly all applications. However a wave-wave analysis would be preferred for applications when the phases of waves are of first interest, such as in the breaking zone.

5.4 XBeach Numerical Model

The XBeach model is a process-based model developed by the Delft University of Technology. It is a two-dimensional, depth-integrated numerical model that simulates the hydrodynamics, sediment transport, and morphological changes of coastal systems. XBeach is a flexible model that can be used to simulate a variety of coastal processes, including wave breaking, bedload transport, and nearshore morphological changes. The model is based on the principles of conservation of mass, momentum, and energy and uses a finite-difference numerical scheme to solve the governing equations. XBeach has been widely used in coastal studies due to its flexibility and accuracy, and it has been applied to a wide range of coastal systems, including estuaries, beaches, and coastal wetlands. The model can be used as a profile model in 1D (Pender et al. 2013), or as an area model in 2D (McCall et al. 2010), and today, there are three modes in which the hydrodynamics can be resolved in XBeach, being:

- **Stationary** – All wave group variations, and thereby all infragravity motions, are neglected, and only the mean motions are included. This type can be applied for modelling morphological changes under moderate wave conditions;
- **Surfbeat** – This in-stationary, hydrostatic mode, is wave group resolving, and is hence also applicable when one is interested in the swash zone processes;
- **Non-hydrostatic** – The non-linear Shallow-Water equations are solved, and hence individual short wave propagation and transformation is resolved.

In our case, we will focus on the **Stationary** mode.

5.4.1 Hydrodynamics

The wave action balance is solved to obtain the wave forcing:

$$\frac{\partial A}{\partial t} + \frac{\partial c_x A}{\partial x} + \frac{\partial c_y A}{\partial y} + \frac{\partial c_\theta A}{\partial \theta} = -\frac{D_w}{\sigma} \tag{2.57}$$

Where A is the wave action, C the wave propagation speed (where the subscripts refer to the $x-$ and $y-$directions, and $\theta-$space), θ is the angle of incidence, D_w the wave

energy dissipation per directional bin and σ the intrinsic wave frequency. The wave action as above (5.5) by:

$$A(x,y,t,\theta) = \frac{S_w(x,y,t,\theta)}{\sigma(x,y,t)} \tag{2.58}$$

In which the Sw is the wave energy density per directional bin. The total wave energy E_H is obtained by integration of the wave energy density Sw over all directional bins:

$$E_H = \int_0^{2\pi} S_w(x,y,t,\theta)\mathrm{d}\theta \tag{2.59}$$

The distribution of the total wave energy dissipation $\bar{D}w$ over all directional bins is calculated proportional to the energy density distribution as follows:

$$D_w(x,y,t,\theta) = \frac{S_w(x,y,t,\theta)}{E_w(x,y,t)}\bar{D}_w(x,y,t) \tag{2.60}$$

The total wave energy dissipation is calculated using a method described by D. J. Roelvink (1993) as the product of the dissipation per breaking event and the fraction of broken waves Qb. The energy dissipation per wave breaking event is assumed to take place over half of the representative wave period T_{rep}, resulting in the following expression for the total, directionally integrated, wave energy dissipation:

$$\bar{D}_w = \alpha \frac{2}{T_{rep}} Q_b E_H \tag{2.61}$$

Where α is a calibration factor and E_w the total wave energy (Equation (5.6)). The fraction of breaking waves Qb is estimated from a Rayleigh distribution (Battjes et al. 1978):

$$Q_b = 1 - \exp\left(-\left(\frac{H_{rms}}{H_{\max}}\right)^n\right) \tag{2.62}$$

Where the root-mean-square wave height H_{rms} is calculated from the wave energy E_H, and the maximum wave height H_{max} is calculated using the breaker index γ (the ratio between the breaking wave height and the water depth, usually given the value 0.88).

$$E_H \sim \frac{1}{8}\rho g H_{rms}^2 \quad \Rightarrow \quad H_{rms} = \sqrt{\frac{8E_w}{\rho g}}, \quad H_{\max} = \gamma_b h \tag{2.63}$$

This closes the set of equations for the wave action balance (Equation (5.4)). From the wave energy, the wave-induced radiation stresses can be determined using linear wave theory. Similar to the wave action balance, a roller balance is solved and coupled to the wave energy balance, where the wave energy dissipation forms a source of energy in

the roller balance. The roller-induced radiation stress is calculated and together with the wave-induced radiation stress they are used to calculate the wave forcing: The flows are calculated using a depth-averaged formulation of the Shallow-Water equations, taking into account wave-induced mass flux and return flows. This Generalized Lagrangian Mean (GLM) formulation uses Lagrangian velocities (Andrews et al. 1978):

$$\frac{\partial u^L}{\partial t} + u^L\frac{\partial u^L}{\partial x} + v^L\frac{\partial u^L}{\partial y} - fv^L - v_h\left(\frac{\partial^2 u^L}{\partial x^2} + \frac{\partial^2 u^L}{\partial y^2}\right) = \frac{T_{sx}}{\rho h} - \frac{T^E_{bx}}{\rho h} - g\frac{\partial \eta}{\partial x} + \frac{F_x}{\rho h} \tag{2.64a}$$

$$\frac{\partial v^L}{\partial t} + u^L\frac{\partial v^L}{\partial x} + v^L\frac{\partial v^L}{\partial y} + fu^L - v_h\left(\frac{\partial^2 v^L}{\partial x^2} + \frac{\partial^2 v^L}{\partial y^2}\right) = \frac{T_{sy}}{\rho h} - \frac{T^E_{by}}{\rho h} - g\frac{\partial \eta}{\partial y} + \frac{F_y}{\rho h} \tag{2.64b}$$

$$\frac{\partial \eta}{\partial t} + \frac{\partial u^L h}{\partial x} + \frac{\partial v^L h}{\partial y} = 0 \tag{2.64c}$$

Where the Lagrangian velocity components (denoted by the superscript L) are the superposition of the Eulerian velocity and the Stokes' drift velocity:

$$u^L = u^E + u^S \quad \text{and} \quad v^L = v^E + v^S. \tag{2.65}$$

In this thesis, we use version 1.23 of XBeach.

5.5 SWAN Numerical Model

SWAN, in its third version, is in stationary mode (optionally non-stationary) and is formulated in Cartesian or spherical coordinates. The unconditional numerical stability of the SWAN model makes its application more effective in shallow water. In SWAN, the waves are described with the two-dimensional spectrum of the wave action density A,

$$A(x, y, \sigma, \theta) = \frac{E(x, y, \sigma, \theta)}{\sigma} \tag{2.66}$$

where x and y are the horizontal components of geographic space, σ is the relative frequency, θ is the wave direction, and E is the energy density.

The spectrum considered in the SWAN model is that of the wave action density $A(\sigma, \theta$) rather than the spectrum of the energy density $E(\sigma, \theta)$. This is because, in the presence of currents for the reasons we mentioned above (non conservation of E_H) (G. B. Whitham 2011). Because wave action propagates in both geographic and spectral space under the influence of genesis and dissipation terms, wave characteristics are described in terms of two-dimensional wave action density. The action density spectrum balance equation relating the propagation term to the effects of the source and sink terms, in Cartesian

coordinates, is (Hasselmann et al. 1973)

$$\frac{\partial A}{\partial t}+\frac{\partial\left(C_x A\right)}{\partial x}+\frac{\partial\left(C_y A\right)}{\partial y}+\frac{\partial\left(C_\sigma A\right)}{\partial \sigma}+\frac{\partial\left(C_\theta A\right)}{\partial \theta}=\frac{S}{\sigma}. \tag{2.67}$$

On the left-hand side of Equation (5.14), the first term represents the local temporal variation of the wave action density, the second and third terms represent the propagation of wave action in the geographical space of velocities C_x and C_y, the fourth term represents the shifting of the relative frequency due to variations in bathymetry (with propagation velocity C_σ) and currents (with propagation velocity C_θ), and the fifth term represents the refraction induced by the combined effects of depth and currents. $C_x, C_y, C_\sigma, C_\theta$ propagation velocities are obtained from linear wave theory. The term in the right-hand side of Equation (5.14) represents processes that generate, dissipate, or redistribute wave energy, and S can be expressed as (Lv et al. 2014)

$$S = S_{in} + S_{wc} + S_{brk} + S_{bot} + S_{n14} + S_{n13} \tag{2.68}$$

where S_{in} is the wind energy input. The dissipation terms of wave energy is represented by the contribution of three terms: the white capping S_{wc}, bottom friction S_{bot}, and depth induced breaking S_{brk}. S_{n14} and S_{n13} represent quadruplet interaction and triad interactions, respectively.

A finite difference scheme is use for each of the five dimensions: time, geographic space, and spectral space made the numerical implementation in SWAN effective. The following guidelines must be followed in order to obtain the discretization adopted at the SWAN model level for numerical computation:

1. time of a constant and identical time step Δt for the propagation term and the source term,

2. geographical space of a rectangular grid with constant spatial steps Δx and Δy,

3. spectral space of a constant directional step $\Delta\theta$ and a constant relative frequency step $\Delta\sigma/\sigma$,

4. frequencies between a fixed minimum maximum values of 0.04 Hz and 1 Hz respectively,

5. the direction θ can also be delimited by the minimum and maximum values θ_{min} and θ_{max} (as an option).

In this thesis, we use version 41.31 of SWAN.

5.6 Hydrodynamic Simulations

In this section, we focus on two types of simulations. The simulations in flume and those in open-sea.

5.6.1 Flume Experiment

For this section, we will concentrate on a reduced number of simulations. We will limit ourselves to simulate the hydrodynamics on two specific cases. The case LIP11D - 1C **S.6** which is a flume experiment. This case is part of the XBeach benchmark (Roelvink et al. 1995) and has allowed the validation of this one. Other models like CROCO (Marchesiello et al. 2022) based their validation on this benchmark. This experiment present hydrodynamic and morphodynamic data. For the second case, we choose a very simple bathymetry: linear. This one is the result of the linear interpolation on the bathymetry LIP11 1C. For these 2 cases, we perform hydrodynamic simulations with the SWAN model **5.5**, XBeach model **5.4**, an extended Shoaling model presented in **3.4** and Shallow-Water model presented in **4.3**. The results are evaluated with the criterion H_{RMSE} which corresponds to the RMSE (root mean square) between experimental and numerical H.
In order to configure our models, we set the domain Ω over 180 m with a uniform subdivision of 180 cells. The incoming wave boundary condition is provided using a JONSWAP wave spectrum (Hasselmann et al. 1973), with a significant wave height of $H_s = 0.6$ m and a peak frequency at $f_p = 5$ s^{-1}. The breaker model of XBeach uses the D. J. Roelvink (1993) formulation, with a breaker coefficient of $\gamma = 0.4$, a power $n = 15$, and a wave dissipation coefficient of 0.5. For the breaker model of SWAN and Shoaling, we simply use the breaker coefficient of $\gamma = 0.4$. The parameter files are present in the appendix **A.1**. The results of LIP11D - 1C and its linear interpolation are in figures **2.8** and **2.9** below.

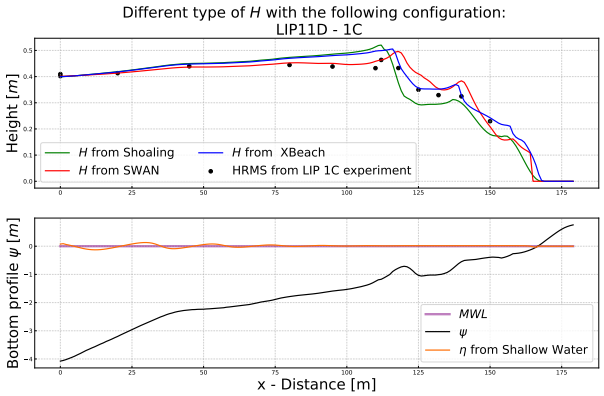

Figure 2.8 – Hydrodynamic results obtained with the Shoaling, SWAN, XBeach and Shallow-Water models. Bathymetric configurations from the LIP 1C channel experiment. Black points, measured HRMS, black bathymetry, green H from extended shoaling (H_{RMSE} = 0.045 m), red H from SWAN (H_{RMSE} = 0.033 m), blue H from XBeach (H_{RMSE} = 0.028 m) and orange from Shallow-Water model.

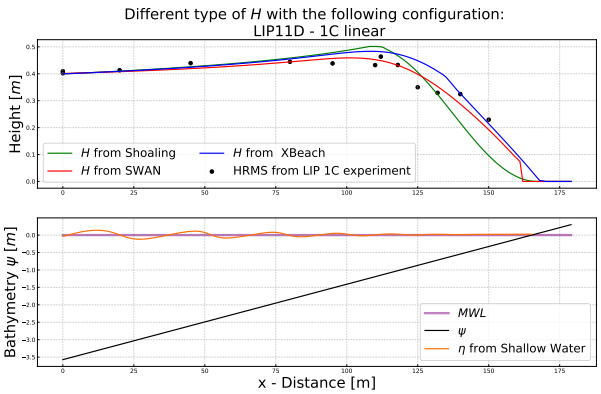

Figure 2.9 – Hydrodynamic results obtained with the Shoaling, SWAN, XBeach and Shallow-Water models. Bathymetric configurations from a linear interpolation of the LIP 1C channel experiment. Black bathymetry, green H from extended shoaling (H_{RMSE} = 0.059 m), red H from SWAN (H_{RMSE} = 0.024 m), blue H from XBeach (H_{RMSE} = 0.043 m) and orange from Shallow-Water model.

We notice that XBeach reproduces best the experimental results (H_{RMSE} = 2.8 cm). However, the 3 results are still very good and very realistic. For the linear profile, we have chosen to leave the experimental points of the previous experiment. The results are surprising because SWAN remains very close to these points (H_{RMSE} = 2.4 cm). We noticed with another case that the points were almost superimposed, whether in experimental or linear bathymetry.

5.6.2 Open-Sea Simulation

For this section, we perform realistic open-sea simulations. These simulations will allow us to introduce a bathymetry set that can be used in our morphodynamic model. We perform simulations on configurations such as linear, convex and concave bathymetry. For these 3 cases, we perform hydrodynamic simulations with the SWAN model **5.5**, XBeach model **5.4**, an extended Shoaling model presented in **3.4** and Shallow-Water model presented in **4.3**.

In order to configure our models, we set the domain Ω over 600 m with a uniform subdivision of 600 cells. The incoming wave boundary condition is provided using a $H_0 = 2$ m parameter, with a wave period $T_0 = 12$ s. The breaker model of XBeach uses the D. J. Roelvink (1993) formulation, with a breaker coefficient of $\gamma = 0.55$, a power $n = 15$, and a wave dissipation coefficient of 0.5. For the breaker model of SWAN and Shoaling, we simply use the breaker coefficient of $\gamma = 0.55$. The parameter files are present in the appendix **A.1**. This gives us the following results:

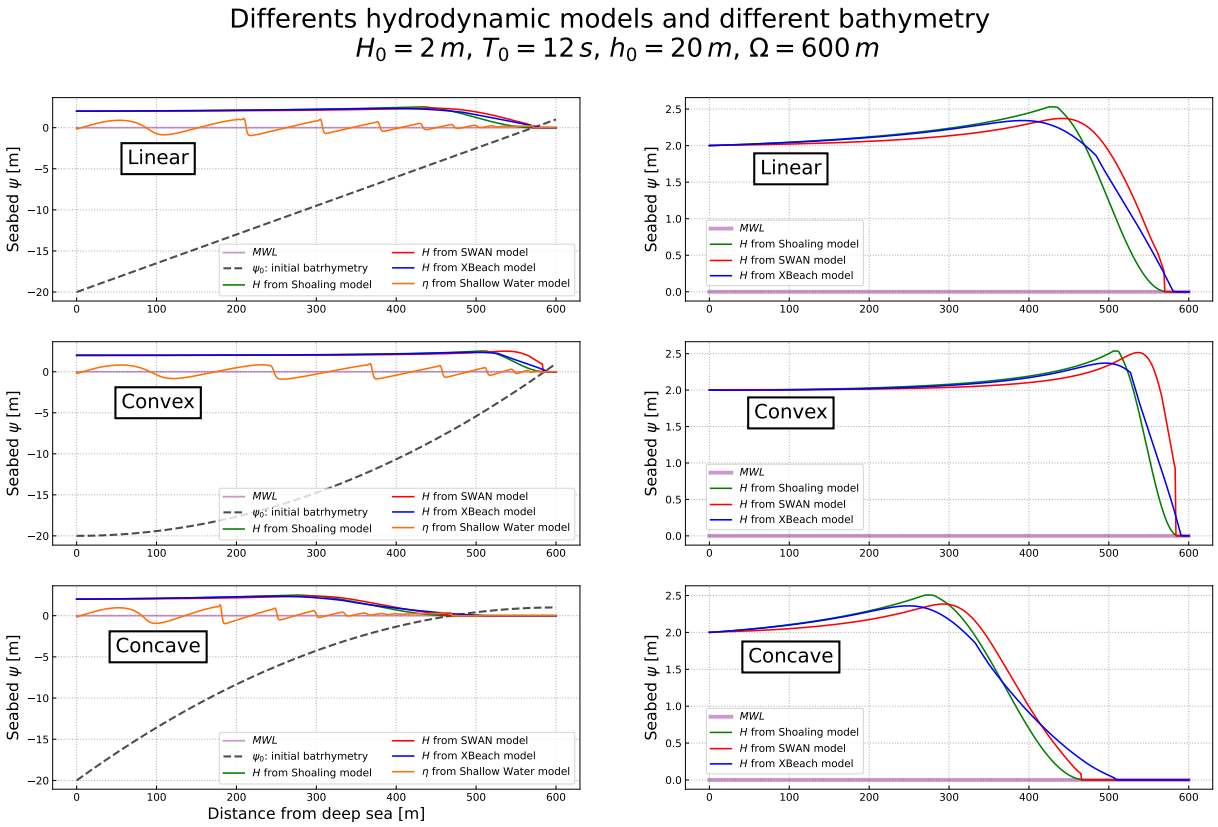

Figure 2.10 – Hydrodynamic results obtained with the Shoaling, SWAN, XBeach and Shallow-Water models. Bathymetric configurations from a linear, convex and concave open-sea configurations. Black bathymetry, green H from extended shoaling, red H from SWAN, blue H from XBeach and orange η from Shallow-Water model.

Also, we notice that the 3 spectral hydrodynamics are relatively close. The extended shoaling model seems to be slightly different from the two others.

6 Conclusion

In this chapter, we have seen the mathematical formalism on which coastal hydrodynamic models are based. We have chosen to present in detail the spectral and temporal resolution models and the way to generate a significant water height H_s. We present more precisely the well known models SWAN, XBeach, REF/DIF and Shallow-Water. Moreover, we have introduced an extended shoaling model which allows us to have correct results at a very low complexity. The hydrodynamic simulations presented for the benchmark (Roelvink et al. 1995) give results very close to the experimental data. Open-sea simulations have also been introduced in order to highlight the versatility of our model.

Chapter key points

- We have introduced the mathematical formalisms of coastal hydrodynamics.
- We design a new hydrodynamic model which we call extended shoalling model.
- We performed simulations of a benchmark: LIP11D-1C with SWAN, XBeach and extended shoaling models.
- We performed simulations on Open-Sea with linear, concave and convexe configuration using SWAN, XBeach, extended shoaling models and Shallow-Water model.